J. Fluid Mech. (1982), *vol.* 120, *pp.* 219–244
Printed in Great Britain

Discrete-vortex simulation of a turbulent separation bubble

By MASARU KIYA, KYURO SASAKI AND MIKIO ARIE
Faculty of Engineering, Hokkaido University, Sapporo, 060, Japan

(Received 26 August 1981 and in revised form 17 November 1981)

The discrete-vortex model is applied to simulate the separation bubble over a two-dimensional blunt flat plate with finite thickness and right-angled corners, which is aligned parallel to a uniform approaching stream. This flow situation is chosen because, unlike most previous applications of the model, the separation bubble is supposed to be strongly affected by a nearby solid surface. The major objective of this paper is to examine to what extent the discrete-vortex model is effective for such a flow. A simple procedure is employed to represent the effect of viscosity near the solid surface; in particular, the no-slip condition on the solid surface. A reduction in the circulation of elemental vortices is introduced as a function of their ages in order to represent the three-dimensional deformation of vortex filaments. An experiment was also performed for comparison purposes.

The calculation yielded reasonable predictions of the time-mean and r.m.s. values of the velocity and the surface-pressure fluctuations, together with correlations between their fluctuating components, over most of the separation bubble. The interrelation between instantaneous spatial variations of the surface-pressure and velocity fluctuations were also obtained. A comparison between the calculated and measured results suggests that, in the real flow, the three-dimensional deformation of vortex filaments will become more and more dominant as the reattachment point is approached.

1. Introduction

The discrete-vortex model is emerging as a powerful method for simulating high-Reynolds-number flows of unsteady nature in two and three dimensions. An excellent review has recently been written by Leonard (1980). Recent applications of the discrete-vortex model to unsteady separated flows past two-dimensional bluff bodies have suggested that the circulation of elemental vortices should be reduced as a function of time in order to obtain a satisfactory agreement between calculated and measured forces acting on the bluff bodies (Sarpkaya & Shoaf 1979; Ashurst 1979*a*; Kiya & Arie 1980; Ashurst, Durst & Tropea 1980; Nagano, Naito & Takata 1981). In these studies, the circulation reduction is introduced mainly because none of the previous methods (see Sarpkaya & Shoaf 1979) can bring about the experimentally measured values of the cancellation of shed vorticity in the near wake. Moreover, none of the methods account for the observed fact that the strength of rolled-up vortices continues to decrease with time or downstream distance. The reduction in circulation may be justified as accounting for the three-dimensional deformation of vortex filaments which would occur in a real flow of high Reynolds number.

The reduction in circulation is inconsistent with an inviscid-flow theorem, which requires that the strength of vortices should remain constant in time. However, if a separated viscous flow in two dimensions is to be modelled by discrete vortices, then the relation $D\omega/Dt = 0$, where ω is the vorticity and t is time, has to be disregarded. Strictly, this may seem to be impermissible. We are, however, of the opinion that the circulation-reduction procedure should be accepted if it is able to reproduce some important features of separated flows to the extent that they are of sufficient accuracy for engineering purposes and can be estimated on a general rather than a particular basis. A compromise between exactness and usefulness should not always be rejected because the prediction of various aspects of turbulent separated recirculating flows at high Reynolds numbers is still uncertain. If some important information can be extracted from the resulting model it may enhance our understanding of the separated flow and at the same time contribute to the development of prediction methods.

Apart from several exceptions, most developers and users of the discrete-vortex model have concentrated on gross features of flow such as vortex patterns, Strouhal number, drag and lift. They fail to show many important flow details such as the time-averaged and r.m.s. values of the fluctuating velocity and pressure in the separated regions. Since accurate measurements of these quantities in recirculating flows are not easy as yet, the value of the discrete-vortex method will be enhanced if it can make predictions with fairly good accuracy. Clements (1973) calculated the distributions of the time-averaged value and amplitude of the velocity fluctuation in the potential-flow region near the separation point of a square-based body. The time-averaged velocity is found to be in tolerable agreement with experiment, whereas the calculated amplitude is less than half the measured one. The mean and fluctuating velocities in the separated region are not given. Clements & Maull (1975) computed the time-averaged velocity distributions in the recirculating region behind a downward-facing step to show that the agreement between their calculation and the experiment of Tani, Iuchi & Kodoma (1961) is fairly good. The fluctuating velocities, however, were not presented at all. Kiya & Arie (1980) made a detailed calculation of the time-averaged and r.m.s. values of the velocity fluctuations in the near wake of a normal flat plate by reducing the circulation of elemental vortices as a function of their ages. Their results are in good agreement with the careful measurements of Bradbury (1976). Kiya & Arie (1980) argue that, unless the circulation reduction is introduced, the good agreement is not obtained. Ashurst (1979*a*) applied the discrete-vortex model to compute the separated flow in symmetric channels that have sudden expansions and in the flow behind a single downward-facing step. An approximate vortex ageing is introduced, and the plane solid wall downstream of the step is treated by creating new vorticity along the wall. The calculated time-mean and turbulent normal and shear stresses are unsatisfactorily predicted except for a few locations downstream of the step.

In passing, a few successful cases without recirculation will be mentioned. Assuming the circumferential velocity field around an elemental vortex to be that of an isolated viscous vortex, Ashurst (1979*b*) simulated the plane turbulent mixing layer to obtain excellent agreement between calculated and measured values of r.m.s. velocity fluctuations and the Reynolds shear stress. The axisymmetric turbulent mixing layer was successfully modelled by the superposition of vortex-ring elements (Acton 1980), which reasonably predicts the time-mean longitudinal velocity profile. Aref & Siggia

(1980) calculated the rolling up of the two-dimensional shear layer by the cloud-in-cell method to obtain the r.m.s. velocities and the Reynolds shear stress, which are much larger than experimental results. We conjecture that the discrete-vortex model, if properly developed further, will be able to reproduce those components of time-mean and fluctuating quantities in turbulent flows caused by two-dimensional or axisymmetric large-scale vortices.

Most of the flows mentioned in the last paragraph (except the cases of Clements & Maull (1975), Ashurst (1979*a*) and Ashurst *et al.* (1980)) are those in which the solid surfaces of the bodies downstream of the separation point have relatively weak effects on the dynamics of the separated region. However, the separation bubbles that remain attached to a solid surface are frequently encountered in engineering applications. The main purpose of this paper is to examine the extent to which the discrete-vortex model is effective in the prediction of the time-mean and fluctuating velocities and pressures in a turbulent separation bubble attached to a solid surface. One considers the separation bubble formed along a side of a two-dimensional, semi-infinite blunt flat plate with finite thickness and right-angled corners which is aligned parallel to a uniform approaching stream. This flow configuration is particularly convenient because the boundary layer at the separation point is so thin that the number of parameters required to describe the upstream-flow conditions is expected to be minimal.

Within the framework of the discrete-vortex model, the solid surface is assumed to influence the behaviour of the separation bubble through two mechanisms. One is the boundary condition that the flow must be along the surface, the other being the effect of viscosity which requires that the velocity at the surface should be zero. The former can easily be satisfied by the introduction of the image vortices, whereas the latter can in principle be effected by the creation of vortices at the surface to maintain the zero-slip condition (Ashurst 1979*a*; Leonard 1980). Because the number of vortices thus created to satisfy the no-slip condition becomes enormous as time advances, computer budgets at present will not necessarily allow such extravagance. Several methods that have been developed to meet this difficulty are discussed by Leonard (1980). A simple alternative procedure to simulate the viscous effect approximately will be proposed in § 2 of the present paper.

In view of the scarcity of the experimental data (Ota & Kon 1974; Ota & Itasaka 1976; Ota & Narita 1978), measurements were also made of the time-mean and fluctuating velocities and pressure in the separation zone.

In § 2 the physical model and the fundamental equations will briefly be presented, together with the values of a few parameters included in the equations. The experimental apparatus and procedure are described in § 3. The calculated and measured results are presented and compared in § 4, where it will be shown that the present discrete-vortex model yields a fairly good prediction of the time-mean and r.m.s. values of the velocity and surface-pressure fluctuations and correlations between them in the separation bubble.

2. Discrete-vortex model

The model considered here is one of the flow past a two-dimensional flat plate with finite thickness and blunt leading edge which is aligned parallel to a uniform approaching stream. The front surface is normal to the approaching stream, and thus the flow

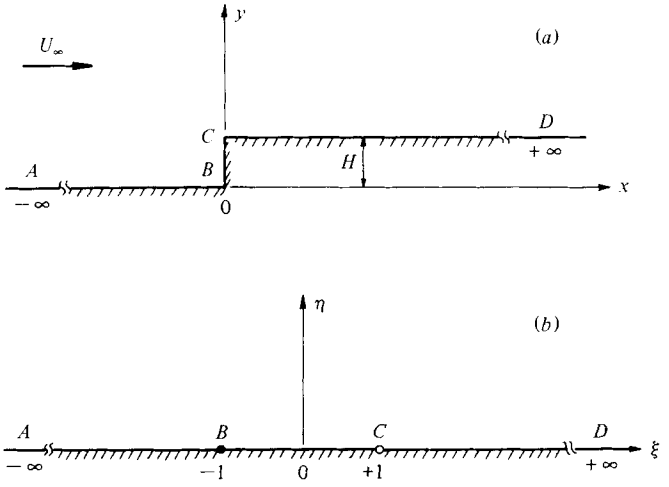

FIGURE 1. (*a*) Physical plane $z(= x+iy)$; (*b*) transformed plane $\zeta(= \xi+i\eta)$.

is assumed to separate at the right-angled corners. Since the behaviour of the separated shear layer from one corner will be insignificantly affected by that from another corner, attention can be concentrated on any one of the two shear layers. Accordingly, the geometry of the body can be chosen as shown in figure 1.

The discrete-vortex model approximates the separated shear layer by an array of line vortices. The motion of the shear layer is then represented by the evolution of the array of line vortices. The velocity of any vortex is the sum of the velocity of the irrotational two-dimensional flow around the body and that induced at the vortex position by all the other vortices. The two velocity components can be obtained by assuming the body to extend to infinity downstream (see figure 1), and then using a Schwartz–Christoffel transformation to project the exterior region of the body (z-plane) into an upper half-plane (ζ-plane) with the boundary of the body along the real axis.

The transformation from the physical z-plane to the transformed ζ-plane, which maps the points $z = 0$ and iH (H being the half-height of the body) into $\zeta = -1$ and $+1$, respectively, is given by

$$z = \frac{H}{\pi}[(\zeta^2-1)^{\frac{1}{2}} - \operatorname{arcosh}\zeta] + iH. \tag{1}$$

The complex potential W_u for the irrotational flow around the body is thus

$$W_u = U_\infty(H/\pi)\,\zeta, \tag{2}$$

where U_∞ is the velocity at upstream infinity. If the number of elemental vortices in the flow field is n, the complex potential W_v of the flow induced by the vortices is given by

$$W_v = \sum_{j=1}^{n} \frac{i\Gamma_j}{2\pi}\{\log(\zeta-\zeta_j) - \log(\zeta-\zeta_j^*)\}, \tag{3}$$

where ζ_j is the location of the jth vortex in the transformed plane, ζ_j^* its complex conjugate, and Γ_j denotes its circulation. The second term in the curly bracket of (3) represents image vortices which are necessary in order to maintain the boundary

condition of zero flow across the surface of the body. The complex potential W for the total flow field is the sum of (2) and (3), i.e. $W = W_u + W_r$.

The velocity field in the physical plane is given by

$$u - iv = \frac{dW}{dz} = \frac{dW}{d\zeta}\frac{d\zeta}{dz}, \tag{4}$$

where u and v are velocity components in the x- and y-directions respectively. The velocity at a vortex point, the kth vortex, say, has to be obtained by differentiating $W - i(2\pi)^{-1}\Gamma_k \log(z - z_k)$ with respect to z, and taking the appropriate limit as $z \to z_k$, the result being

$$u_k - iv_k = U_\infty + \left\{ \sum_{\substack{j=1 \\ j \neq k}}^{n} \frac{i\Gamma_j}{2\pi}\frac{1}{\zeta_k - \zeta_j} - \sum_{j=1}^{n} \frac{i\Gamma_j}{2\pi}\frac{1}{\zeta_k - \zeta_j^*} - \frac{i\Gamma_k}{4\pi}\frac{1}{\zeta_k^2 - 1} \right\} \Big/ \left(\frac{dz}{d\zeta}\right)_{\zeta=\zeta_k}. \tag{5}$$

The position of each vortex was advanced during a small time interval δt by a second-order scheme

$$z_k(t + \delta t) = z_k(t) + \tfrac{1}{2}\{3(u_k + iv_k)_t - (u_k + iv_k)_{t-\delta t}\}\,\delta t. \tag{6}$$

One of the most central assumptions of the discrete-vortex model is the choice of the circulation and location of the vortices introduced in the flow near the separation line. In this paper a technique similar to that of Evans & Bloor (1977) was employed. In order to satisfy the Kutta condition at the edge $z_e\,(= iH)$, there must be a stagnation point at $\zeta = 1$ in the transformed plane. Thus the strength of the nascent vortices is such that

$$(dW/d\zeta)_{\zeta=1} = 0. \tag{7}$$

It is assumed that the width of the separated shear layer at the edge is ϵ. The rate at which vorticity is shed downstream from the separation point is then given by

$$\frac{\Gamma_n}{\delta t_v} = \frac{1}{2}\left|\frac{dW}{dz}\right|^2_{z=z_s}, \tag{8}$$

where Γ_n is the strength of the nascent vortex at an arbitrary time t, δt_v is the time interval between the introduction of the nascent vortices, and z_s is the point $i(H + \epsilon)$. The position of the nascent vortex is assumed to be $z_n = i(H + \frac{1}{2}\epsilon)$. The equations (7) and (8) thus determine the values of Γ_n and ϵ at each calculation step. The solution procedure employed at this work was as follows.

(i) An approximate value of ϵ, say $\epsilon^{(0)}$, was assumed. The value of ϵ at the last step may be utilized as $\epsilon^{(0)}$. In this calculation $\epsilon^{(0)} = 0{\cdot}1H$ was employed as an initial value for all steps.

(ii) Assuming that the strength of the nascent vortex was, to the zeroth-order approximation $\Gamma_n^{(0)}$, equal to that of the last nascent vortex or that of the one most recently obtained, the velocity at the point $z_s = i(H + \epsilon)$ was calculated from (4).

(iii) This velocity determined a new strength of the nascent vortex, say $\Gamma_n^{(1)}$, in conjunction with (8).

(iv) A new value of ϵ, say $\epsilon^{(1)}$, can be obtained from (7) so that the Kutta condition is satisfied. If the condition

$$|\epsilon^{(1)} - \epsilon^{(0)}| \leqslant 0{\cdot}002H, \tag{9}$$

was fulfilled, $\Gamma_n^{(1)}$ and $\epsilon^{(1)}$ were employed as the required values of Γ_n and ϵ respectively.

(v) If (9) was not satisfied, another approximate value of ϵ was obtained from $\epsilon^{(0)}+\alpha(\epsilon^{(1)}-\epsilon^{(0)})$, where α is a parameter introduced to secure the convergence. In this calculation $\alpha = 0{\cdot}3$ was employed. Then one returned to (ii) to repeat the calculation until (9) was satisfied. In this case, $\Gamma_{\mathrm{n}}^{(0)}$ of (ii) should be replaced by $\Gamma_{\mathrm{n}}^{(1)}$.

(vi) If the calculation did not converge after thirty iterations, ϵ was set equal to $0{\cdot}1H$. Moreover, when ϵ became larger than $0{\cdot}4H$, or negative, $\epsilon = 0{\cdot}4H$ was employed rather arbitrarily. In the present calculation, the latter procedure was necessary for about 15 % of the time steps during $U_\infty t/H = 20$–50, t being the time from the start of the flow.

It should be remarked that the present method, unlike that of Evans & Bloor (1977), incorporates the velocity induced by the nascent vortex itself into the determination of its strength by (8).

The circulation of every vortex was reduced according to the law

$$\frac{\Gamma(t)}{\Gamma_0} = 1-\exp\left[-\frac{a^2 Re}{4(U_\infty t/H)}\right], \tag{10}$$

where Γ_0 is the initial strength, $\Gamma(t)$ is the circulation at time t (age of the vortex), a is a constant, and Re denotes the Reynolds number $U_\infty H/\nu$, ν being the kinematic viscosity of fluid. In order to fix the decay law, one need only assign the value of the product $a^2 Re$, which was found to be about 60 for a fairly good overall agreement between calculation and experiment to be obtained in the present case. An optimum value of $a^2 Re$ will depend on the type of flows to be considered. The decay law (10) was employed simply because it is the exact solution of the Navier–Stokes equations for a single rectilinear viscous vortex if a is replaced by the radial distance measured from the centre of the vortex. It may be noted that (10) is a representation of the growth of the three-dimensionality in the flow, so that any decay law which works should be said to be appropriate. In this paper, no attempt was made to compare various decay laws (Sarpkaya & Shoaff 1979; Nagano *et al.* 1981) in order to find the most appropriate one, if any.

The viscosity of fluid requires that the velocity on a stationary solid surface should be zero. If the no-slip condition is to be effected by the creation of vortices at the surface (see § 1), the sign of these vortices is opposite to that of the vortices that represent the separated shear layer. The introduction of the former vortices will change the time-mean velocity profile in the separation bubble, and thus its displacement thickness, compared with the case where only the latter vortices are present. From the equation of continuity, the transverse velocity component v_δ at the edge of the separation bubble is given by

$$v_\delta = U_\infty \frac{d\delta^*}{dx}, \tag{11}$$

where δ^* is the displacement thickness. Conceptually one assumes that the displacement thickness δ^* consists of two contributions, i.e. the velocity defect due to the shear-layer vortices (δ_{s}^*) and that due to the no-slip vortices (δ_{v}^*). The former is in principle automatically represented by the evolution of the vortices, whereas the latter is simulated by an approximate means in this study. To a rough approximation, δ^* is assumed to be the sum of the two contributions, i.e.

$$\delta^* = \delta_{\mathrm{s}}^* + \delta_{\mathrm{v}}^*. \tag{12}$$

From (11) the velocity v_δ can be written as

$$v_\delta = v_\delta^{(\mathrm{s})} + v_\delta^{(\mathrm{v})}, \tag{13}$$

where

$$v_\delta^{(\mathrm{s})} = U_\infty \frac{d\delta_{\mathrm{s}}^*}{dx}, \tag{14}$$

$$v_\delta^{(\mathrm{v})} = U_\infty \frac{d\delta_{\mathrm{v}}^*}{dx}. \tag{15}$$

Equation (15) seems to suggest that the effect of the no-slip vortices may be represented by adding a transverse velocity $v_\delta^{(\mathrm{v})}$ to the velocity that exists originally at the position of every vortex in the vicinity of the edge of the separation bubble. Since an *a priori* estimation of $v_\delta^{(\mathrm{v})}$ is difficult, it is assumed to be a constant. Moreover, for the sake of simplicity, every vortex in the flow field is endowed with the same velocity without regard to its y-co-ordinate. This approximation yields a bodily displacement of the shear layer towards the transverse direction. We believe that this is not necessarily a bad approximation to the viscous effect. In this work $v_\delta^{(\mathrm{v})} = 0{\cdot}0125U_\infty$ was finally employed.

Vortices occasionally approached so close to the side of the blunt body that the presence of the image vortices in the body caused them to have unreasonably large velocities. To prevent this occurring, vortices that approached the wall nearer than $0{\cdot}02H$ were removed from the flow field. Monitoring of the computations revealed that this process involved, on average, the removal of about 2 % of all the vortices introduced into the flow.

Since a considerable number of vortices exist in the flow field, it is probable that some vortices attain small separation and produce large velocities at each other's positions because of the absence of viscosity. This was avoided by the use of the cut-off vortex originally suggested by Chorin (1973), i.e.

$$\psi_\sigma = \begin{cases} (2\pi)^{-1}\,\Gamma \log r & (r > \sigma), \\ (2\pi)^{-1}\,\Gamma(r/\sigma) & (r \leqslant \sigma), \end{cases} \tag{16}$$

where ψ_σ is the stream function of the vortex, Γ the circulation, r the distance measured from the centre of the vortex, and σ denotes the cut-off radius.† Chorin (1973) argues that results of calculation based on (16) are not sensitive to the exact choice of ψ_σ for $r \leqslant \sigma$. The cut-off radius σ was chosen to be $0{\cdot}05H$ in view of the values of similar parameters employed by previous investigators (see Kiya & Arie 1977).

The time step δt for the movement of vortices was taken as $0{\cdot}16H/U_\infty$. Although this time step may not be small enough to represent the real vortex structures immediately downstream of the separation point, it was sufficiently small to simulate the gross flow structure over a major part of the separation bubble. In order to keep the computation time within reasonable bounds, the time interval δt_{v} between the introduction of the nascent vortices was taken as $2\delta t\,(= 0{\cdot}32H/U_\infty)$. Moreover, vortices that passed the vertical line $x = 25H$ were simply removed from the computation. This assumes that there is negligible transport of vorticity in the negative x-direction

† Dr D. Maull suggests that the effect of viscosity can be best represented by an equation like (16) with σ as a function of time and Reynolds number. Such an attempt is made by Nagano *et al.* (1981).

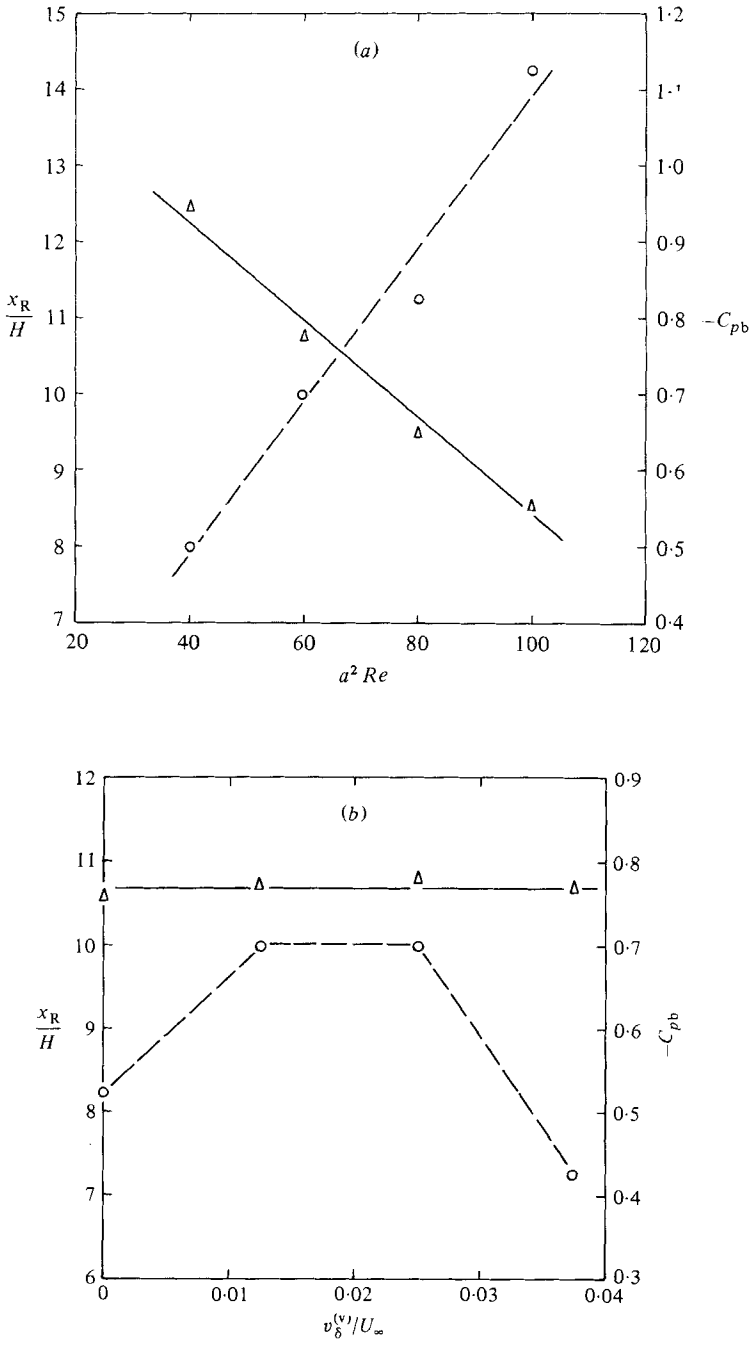

FIGURE 2(*a*, *b*). For caption see facing page.

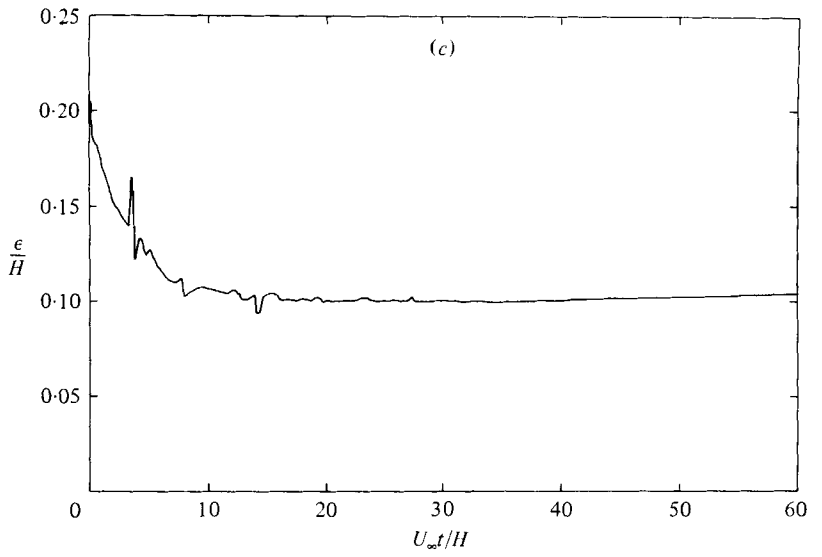

FIGURE 2. Change of the position of the reattachment point x_R and the surface-pressure coefficient $-C_{pb}$ at $x/H = 0{\cdot}5$ as functions of (*a*) a^2Re ($v_\delta^{(v)}/U_\infty = 0{\cdot}0125$) and (*b*) $v_\delta^{(v)}/U_\infty$ ($a^2Re = 60$); and (*c*) change of ϵ with respect to time for $a^2Re = 60$ and $v_\delta^{(v)}/U_\infty = 0{\cdot}0125$. Lines for visual aid only.

at $x = 25H$. Since the calculated time-mean reattachment point existed at $x \simeq 9{\cdot}3H$, this assumption may be justified.

A large number of preliminary calculations were performed to find the optimum values of the various parameters mentioned above. The fluid was assumed to be set in motion impulsively from rest in an otherwise stationary fluid. Figures 2 (*a*) and (*b*) show the location of the reattachment point x_R and the surface-pressure coefficient (see (17)) at $x/H = 0{\cdot}5$ as functions of the decay parameter a^2Re and the additional normal velocity $v_\delta^{(v)}$ respectively. The values of the other parameters were the same as those mentioned previously. Since the integration to obtain the time-mean values was made over a comparatively short time interval $(83 \sim 93)H/U_\infty$ after the start of flow, they are a little different from the corresponding values for much longer time of integration, which will be shown in § 4. The results compiled in figures 2 (*a*, *b*), however, can indicate the general trends of change of the above two quantities with the parameters a^2Re and $v_\delta^{(v)}$. It is interesting to note that the surface-pressure coefficient in the vicinity of the separation point is almost independent of $v_\delta^{(v)}$, although this velocity has a significant effect on the separation-bubble length. Figure 2 (*c*) shows the change of ϵ with respect to time in an early stage of the development of flow. Very little change of ϵ was observed once the flow became statistically stationary, its value being almost equal to $0{\cdot}1H$. In this sense, a fixed distance ϵ (e.g. Clements 1973) is supposed to give reasonable results if the values of ϵ and other parameters are chosen appropriately. The important thing is that the number of disposable parameters can be reduced by employing the present procedure. This gives us a great advantage when the discrete-vortex model is to be applied to oscillating bodies.

It may be worthwhile to make a comment on the role of the disposable parameters. Since the discrete-vortex model is essentially an inviscid model, some empiricism has to be introduced to simulate the actual separation bubbles which are viscous and

dissipative in nature. Primary parameters in the present model are the decay parameter $a^2 Re$ and the additional transverse velocity $v_\delta^{(v)}$, other parameters influencing the results insignificantly. These two parameters have been determined so that the time-mean surface pressure immediately downstream of the separation point and the time-mean reattachment point agree with the result of Ota & Itasaka's (1976) experiment. Our philosophy is that, if we can obtain much more information than the input from the model, its existence can be justified. One may recall here the free-streamline theory or the wake model for bluff bodies in which the base pressure and the boundary-layer separation point have to be given experimentally in order to obtain the surface-pressure distribution and streamline patterns outside the wake region.

Final computation was performed from $U_\infty t/H = 0$–300, which corresponds to 1875 time steps. The fluid was assumed to be set in motion impulsively from rest. The resulting location, circulation and velocity of all the vortices in the flow field at each time step were recorded on magnetic disk memory for later use. The vortex patterns and the waveforms of the fluctuating velocity and pressure at a few typical positions seemed to be statistically stationary in the range $U_\infty t/H \geqslant 80$, so that various averaging of the fluctuating quantities were obtained by integration from $U_\infty t/H = 88$ to 288.

On the assumption that all streamlines come from upstream infinity, the pressure p was calculated from the Bernoulli equation

$$C_p \equiv \frac{p-p_\infty}{\frac{1}{2}\rho U_\infty^2} = 1 - \frac{2}{U_\infty^2}\frac{\partial \phi}{\partial t} - \frac{1}{U_\infty^2}\left|\frac{dW}{dz}\right|^2, \tag{17}$$

where C_p is the pressure coefficient, p_∞ the pressure of the free stream, ρ the density of fluid and ϕ implies the velocity potential. The unsteady term $\partial\phi/\partial t$ was evaluated from

$$\begin{aligned}\partial\phi/\partial t &= \mathscr{R}(\partial W/\partial t)\\ &= \mathscr{R}\left\{\sum_{j=1}^{n}\frac{i\Gamma_j}{2\pi}\left(-\frac{\partial\zeta_j/\partial t}{\zeta-\zeta_j}+\frac{\partial\zeta_j^*/\partial t}{\zeta-\zeta_j^*}\right)\right\},\end{aligned} \tag{18}$$

$$\frac{\partial\zeta_j}{\partial t} = \frac{\pi}{H}\left(\frac{\zeta_j+1}{\zeta_j-1}\right)^{\frac{1}{2}}\left(\frac{dW}{dz}\right)_j. \tag{19}$$

In (18) a term proportional to $\partial\Gamma_j/\partial t$ was omitted because (17) is originally obtained for potential flows of inviscid fluids in which the circulation of vortices remains unchanged (Kelvin's law of the conservation of vorticity). We are of the opinion that the omission of this term is necessary if (17) is to be utilized to calculate the pressure. Moreover, even if the decay law (10) is fairly good, it may not necessarily be a good approximation to an actual time derivative of the strength of vortices. At present one has little information about how the exact functional form of the time derivative should be. The appropriateness of the pressure thus obtained has to be determined by comparison with experiments. Finally, if a position at which the pressure was to be calculated was nearer to a vortex than the cut-off radius, the term proportional to the time derivative of its position was removed from (18). This seems to be reasonable because elemental vortices introduced in this paper are different from potential line vortices within the cut-off radius and thus the term concerned is no longer meaningful.

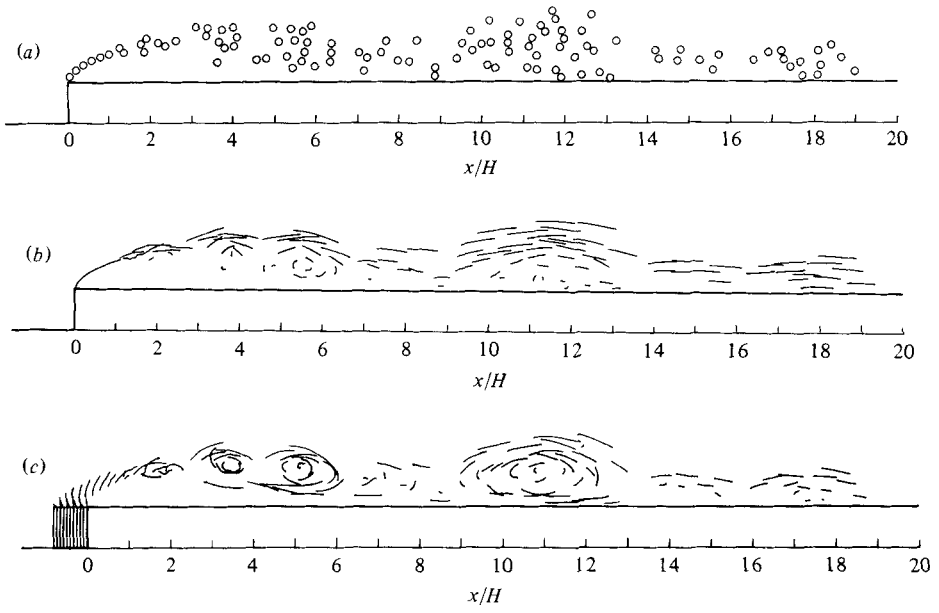

FIGURE 3. (*a*) Distribution of elemental vortices at the time $U_\infty t/H = 281{\cdot}1$ from the start of flow, when the flow is statistically stationary; (*b*) trajectories of vortices during $U_\infty t/H = 280{\cdot}6$–$281{\cdot}6$ with respect to a co-ordinate fixed to the plate; and (*c*) trajectories of vortices during $U_\infty t/H = 280{\cdot}3$–$281{\cdot}9$ with respect to a co-ordinate moving with the velocity $0{\cdot}5U_\infty$ in the downstream direction. Note that several large vortex clouds are evident in (*c*).

3. Experiment

Experiments were carried out in an open-return, low-speed air tunnel with a working section 40 cm high, 20 cm wide and about 1 m long. The tunnel allows speeds up to 24·0 m/s to be obtained through the empty working section. The free-stream turbulence level was 0·3 % at the speed of 20·0 m/s.

The blunt flat plate tested, which was manufactured from acrylic resin plates, was 20 mm thick (H = 10 mm), 50·1 cm long and 20 cm wide, and its leading edge was right-angled. The plate spanned the air tunnel horizontally along its centre line, thus having an aspect ratio of 10. The leading edge of the plate was situated at a distance 50 cm downstream of the beginning of the working section. No end plates were used. An exact alignment of the plate was found by matching pressures recorded on tappings located at the upper and lower surfaces of the plate 5·5, 11·0 and 27·0 cm from the leading edge. A number of pressure taps of 0·7 mm diameter were fitted along the lower side of the plate at the mid-span, the distance between consecutive taps being mostly 5 mm, in order to measure the time-averaged surface-pressure distribution.

The tunnel-wall blockage ratio originally amounted to 5 %, so that it was felt safe to reduce the blockage effect. For this purpose the co-ordinates of a few blockage-free streamlines in the vicinity of the test-section walls were computed by a wake-source model in conjunction with a shape of the separation bubble and the distribution of the displacement thickness along a blunt flat plate measured by Ota & Itasaka (1976). False boundaries of acrylic resin sheet were then introduced along the ceiling and floor of the test section; they were curved according to the blockage-free streamline,

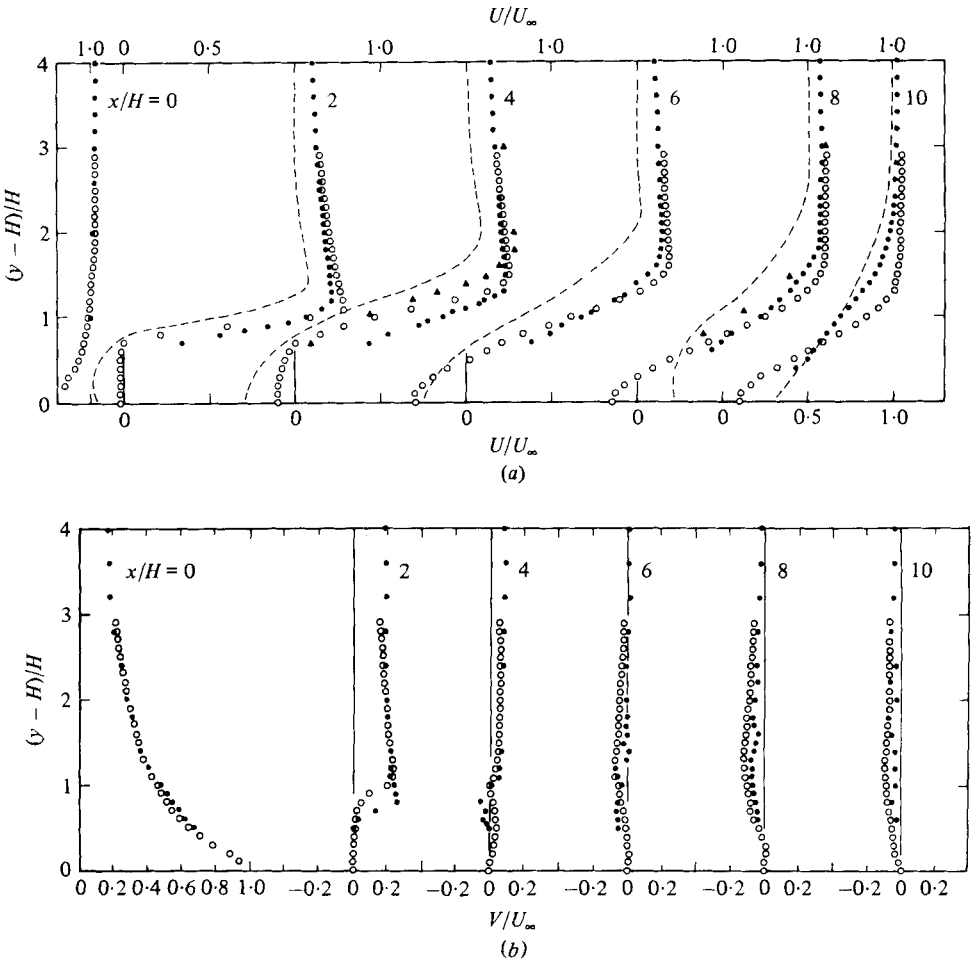

FIGURE 4. Profiles of (*a*) longitudinal and (*b*) normal components of the time-mean velocity in the separation bubble. ○, calculation with $\sigma/H = 0{\cdot}05$; ●, present experiment; ▲, experiment by Ota & Kon (1974); – – –, experiment by Ota & Itasaka (1976).

flared by an amount equal to the displacement thickness of the boundary layer along the tunnel walls, and smoothly joined to the bell entrance of the test section.

The time-averaged and fluctuating velocities in the separation bubble were measured by a constant-temperature hot-wire anemometer using a single-wire technique. The static pressure distribution in the flow was obtained by a static tube of 1·0 mm diameter with the aid of a Betz manometer. These probes were mounted separately on a traversing mechanism outside the tunnel. This allowed the position of the probes to be adjusted within an accuracy of 0·1 mm.

Pressure fluctuations on the surface of the plate were detected by a semiconductor strain-gauged transducer which was mounted inside the plate with a small cavity between a pressure tap of 0·7 mm diameter and the diaphragm of the transducer. This pressure transducer was calibrated against a standard condenser microphone by means of sound waves of various frequencies generated by a loud-speaker. The gain factor was found to be $1 \pm 0{\cdot}1$ up to 450 Hz, with negligibly small phase shift.

The root-mean-square value of the pressure fluctuation was obtained by a true r.m.s. meter. The longitudinal velocity and surface-pressure fluctuations were recorded simultaneously on two channels of an analogue tape recorder (KYOWA R-520A) and were later analysed on a digital signal processor (SANEI 7T074) to give their auto- and cross-correlations. A careful calibration showed that no sensible phase lag existed between the outputs of the hot-wire probe and the pressure transducer.

Finally, the flow pattern on the plate surface was visualized with the aid of titanium oxide suspended in a mixture of light oil, liquid paraffin and silicone oil.

4. Results and discussion

4.1. *Calculated flow patterns*

In order to show general appearance of the separation bubble simulated by the present discrete-vortex model, figure 3 presents the vortex patterns at certain time steps at which the simulated flow in the separation bubble was in the statistically stationary state of fluctuation. Figure 3(*a*) is the location of the elemental vortices. Figures 3(*b*) and (*c*) are the trajectories of the vortices during a short time interval $1{\cdot}60H/U_\infty$ with reference respectively to a co-ordinate fixed to the plate and to one moving in the downstream direction with a velocity $0{\cdot}5U_\infty$ relative to the plate. Figure 3(*c*) shows clearly that several vortex clouds are formed in the separated shear layer and coalesce to form larger and larger vortex clouds which are subsequently swept downstream. Although not exactly periodic, this process occurred from time to time. It may be noted that no artificial device is employed in the present calculation to initiate fluctuations in the flow field.

4.2. *Time-mean velocities and pressure*

The computed distributions of the time-mean velocities U and V are compared with the measured ones in figure 4. Here V and U denote the velocity components in the x- and y-directions respectively. Since the interpretation of hot-wire signals in highly turbulent regions with low time-mean velocity is generally difficult, the data are not shown within a dividing streamline of the separation bubble. The agreement between the calculation and the present experiment is seen to be reasonable only in the region well above the dividing streamline. Moreover, the distribution of U in the vicinity of the stagnation point, which is located at $x/H = 9{\cdot}3$ in this calculation, is poorly predicted. The measurement of Ota & Itasaka (1976) is generally in poor agreement with the above results. Their longitudinal velocity at the outer edge of the shear layer seems to be too low to give the level of the observed negative surface pressure immediately downstream of the separation point. Moreover, the time-mean streamline pattern (figure 5 of their paper) is inconsistent with the velocity profile at a certain section, so that their velocity distribution should be taken with reserve.

The time-mean output of a single hot wire aligned normal to the plane of the flow (the (x, y)-plane) measures the time-mean value Q of the quantity q, where

$$q = [(U+u')^2+(V+v')^2]^{\frac{1}{2}}; \tag{20}$$

u' and v' are the fluctuating velocity components in the x- and y-directions. It may be noted that the effects of heat losses due to the natural convection and the velocity component along the wire axis have been disregarded in (20). Since Q can be measured

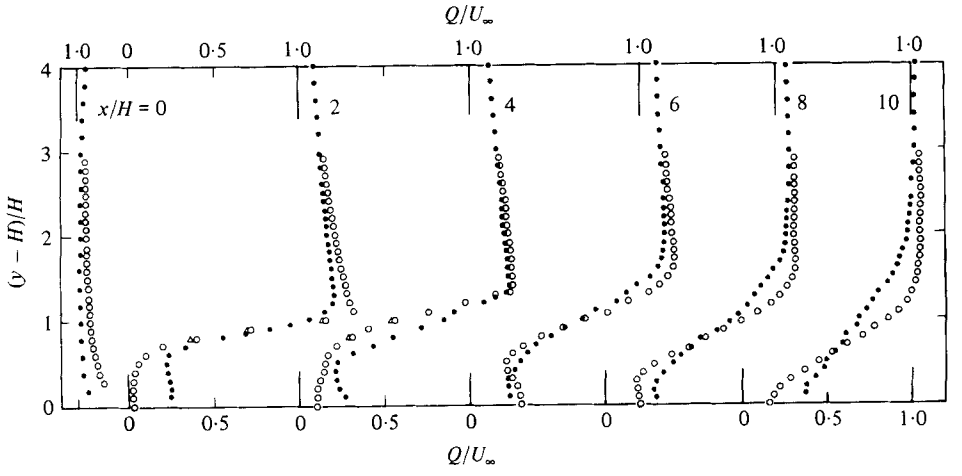

FIGURE 5. Profile of the time-mean value Q of the velocity q defined by (20). ○, calculation with $\sigma/H = 0{\cdot}05$; △, calculation with $\sigma/H = 0{\cdot}075$; ●, present experiment.

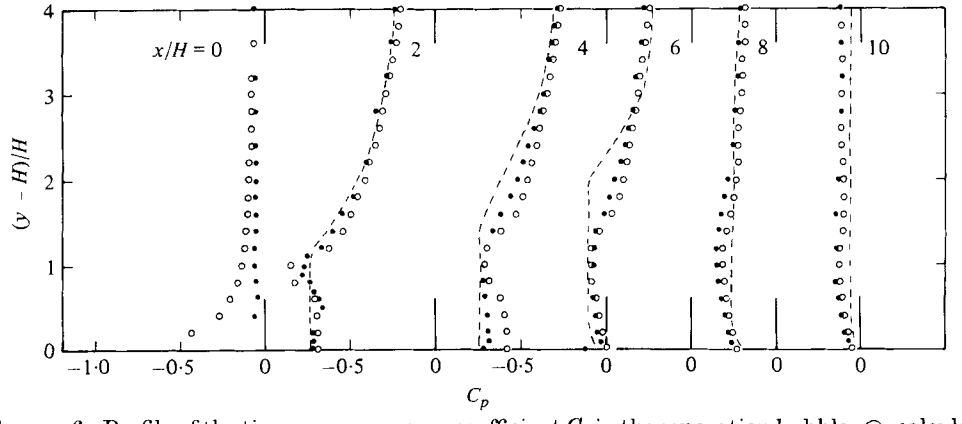

FIGURE 6. Profile of the time-mean pressure coefficient C_p in the separation bubble. ○, calculation with $\sigma/H = 0{\cdot}05$; ●, present experiment; – – –, experiment by Ota & Itasaka (1976).

much more accurately than U or V, its distribution in the separation bubble could be compared with the calculated one in order to examine the extent of accuracy of the present discrete-vortex model. The result is shown in figure 5. The agreement between the calculation and experiment seems to be fairly good except for the region of very low values of Q.

The distribution of the time-mean static pressure P in the flow field is presented in figure 6 in the form of the pressure coefficient $C_p(=(P-p_\infty)/\frac{1}{2}\rho\, U_\infty^2)$. For later convenience, the fluctuating pressure component is denoted by p'. The discrete-vortex model reproduces the experimental results fairly well except for the section $x/H = 0$, where the static-pressure measurement may be prone to large errors near the edge because of large flow curvature. Figure 7 shows the pressure distribution along the plate surface. The prediction is again fairly reasonable.

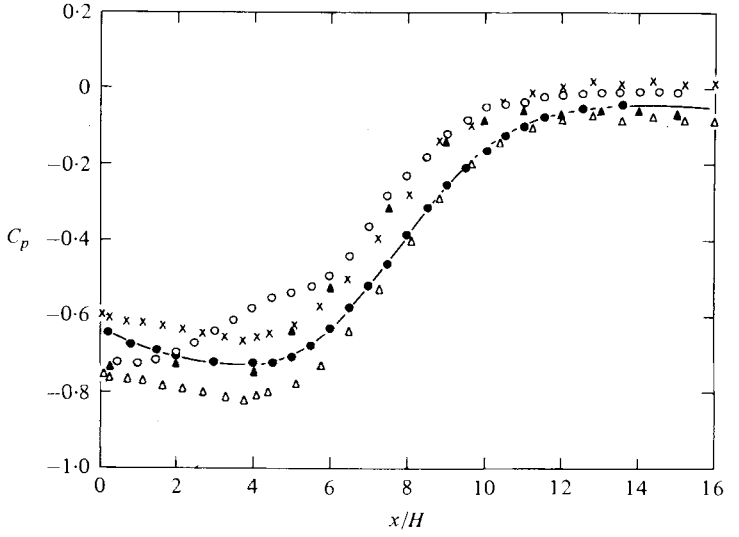

FIGURE 7. Time-mean pressure distribution along the surface of the plate. ○, calculation with $\sigma/H = 0{\cdot}05$; ●, present experiment; ▲, experiment by Ota & Itasak (1976); uncorrected (△) and corrected (×) data (with end plates) of Hillier & Cherry (1981). Line for visual aid only.

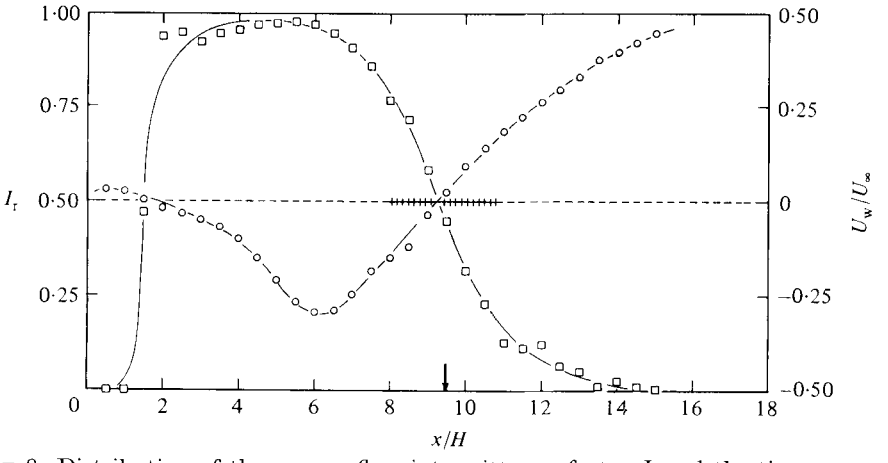

FIGURE 8. Distribution of the reverse-flow intermittency factor I_r and the time-mean surface velocity U_w along the surface of the plate. —□—, I_w; —○—, U_w, calculation with $\sigma/H = 0{\cdot}05$; ↓, time-mean reattachment point in the present experiment; ▮▮▮▮▮▮▮▮, Ota & Itasaka's (1976) reattachment region.

4.3. *Reverse-flow intermittency and reattachment point*

The point where the separated shear layer reattaches on the plate surface moves intermittently back and forth owing to the formation and subsequent downstream shedding of large-scale vortices in the separation bubble. The time-mean reattachment point should thus be defined as a point where the fraction of time I_r during which the flow moves upstream near the plate surface takes the value of 0·5. This reverse-flow intermittency I_r can be easily obtained in the discrete-vortex model, whereas the directional insensitivity of a hot-wire probe prohibits I_r from being obtained experimentally, so that direct comparison between calculation and experiment is not possible.

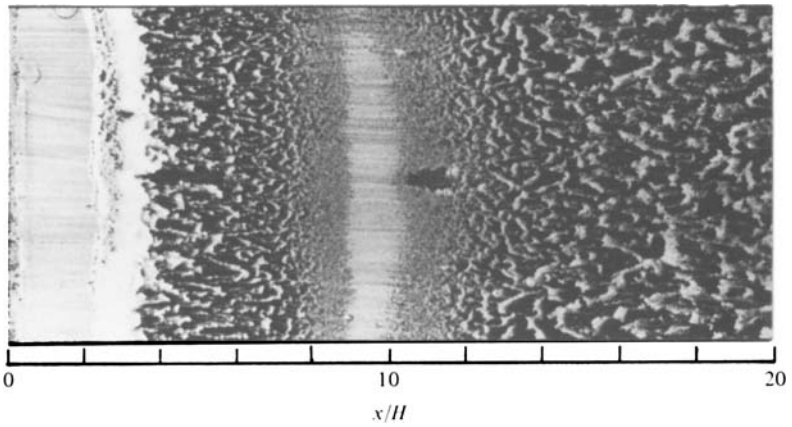

FIGURE 9. Surface-flow pattern.

Figure 8 shows the calculated distribution of I_r on the plate surface together with the calculated time-mean surface velocity U_w. The points where $I_r = 0{\cdot}5$ and $U_w = 0$ are seen to be exactly coincident and located at $x/H = 9{\cdot}3$.

A few interesting features of the $I_r \sim x/H$ curve should be mentioned. Firstly, the reverse-flow intermittency is always less than unity in the time-mean separation bubble. This is also the case, even at the point where the time-mean reverse velocity on the plate surface attains a maximum. Secondly, with decreasing x/H, I_r falls rapidly to zero in the region $x/H \gtrsim 2{\cdot}0$, where the surface velocity becomes positive, although its absolute value is extremely low. This fact strongly suggests that a secondary separation bubble is formed in this region. The surface flow pattern shown in figure 9 is not necessarily inconsistent with the existence of the secondary bubble, because it indicates that the longitudinal velocity in the vicinity of the plate surface is very low in the region $x/H \lesssim 2{\cdot}0$ and that an accumulation of displaced oil occurs over a short distance downstream of $x/H \simeq 2{\cdot}0$.

4.4. *Velocity and pressure fluctuations*

The r.m.s. values of the fluctuating velocity components are shown in figures 10 and 11 as functions of the normal distance from the plate at several downstream sections. The results of Ota & Narita (1978) and the present experiment are also included for the purpose of comparison. Ota & Narita's data on the r.m.s. velocities show that their maxima appear at positions more remote from the plate than the case of the present experiment. This corresponds to a higher location of the separated shear layer in their experiment, as will be seen in the time-mean longitudinal velocity profile (see figure 4*a*). The distributions of the r.m.s. velocities are observed to be tolerably well predicted, except for the region near the reattachment point.

In order to demonstrate the effect of the cut-off radius on the fluctuating quantities, figures 10 and 11 include the calculated results for $\sigma/H = 0{\cdot}075$, all the other parameters being maintained to be the same. The r.m.s. velocities for $\sigma/H = 0{\cdot}075$ are only slightly less than those for $\sigma/H = 0{\cdot}05$, except for the region in the vicinity of the separation point, where the reduction is a little larger. This may imply that the r.m.s. velocities a little downstream of the separation point are governed mainly by

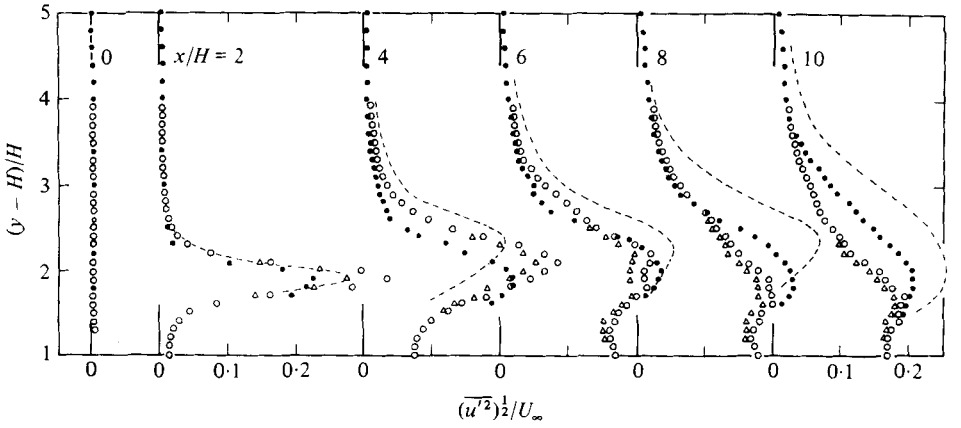

FIGURE 10. Distribution of the r.m.s. longitudinal velocity in the separation bubble. ○, calculation with $\sigma/H = 0{\cdot}05$; △, calculation with $\sigma/H = 0{\cdot}075$; ●, present experiment; – – –, experiment of Ota & Narita (1978). Note that the r.m.s. velocity is sensitive to the cut-off radius in regions where the separated shear layer is thin, see the result for $x/H = 2$.

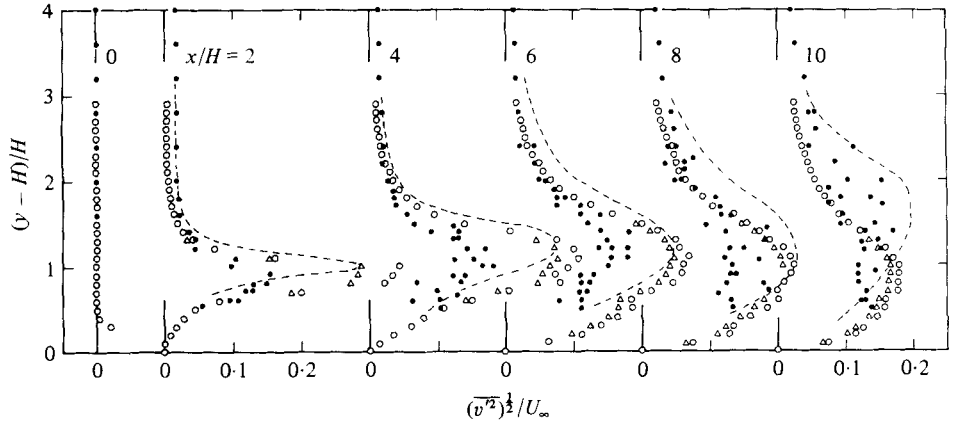

FIGURE 11. Distribution of the r.m.s. normal velocity in the separation bubble. ○, calculation with $\sigma/H = 0{\cdot}05$; △, calculation with $\sigma/H = 0{\cdot}075$; ●, present experiment; – – –, experiment of Ota & Narita (1978). Note that the r.m.s. velocity is sensitive to the cut-off radius in regions where the separated shear layer is thin, see the result for $x/H = 2$.

individual vortices passing near a point where they are calculated, whereas at positions further downstream the r.m.s. velocities are determined by the velocity fluctuations associated with large vortex clouds.

As suggested previously, the fluctuating component of a hot-wire output (normal to the plane of mean flow) in highly turbulent regions can approximately be interpreted as the fluctuating component q' of the quantity q. Then the computed distribution of $(\overline{q'^2})^{\frac{1}{2}}/U_\infty$ is compared with the measured one in figure 12. They are seen to be in tolerable agreement. It may be worth noting that $(\overline{q'^2})^{\frac{1}{2}}$ is only a little different from $(\overline{u'^2})^{\frac{1}{2}}$ in the discrete-vortex calculation, although their time-mean counterparts Q and U are rather different from each other in the separation bubble.

The Reynolds shear stress is plotted in figure 13 in a dimensionless form $-\overline{u'v'}/U_\infty^2$. In this case the discrete-vortex prediction is rather discouraging because the com-

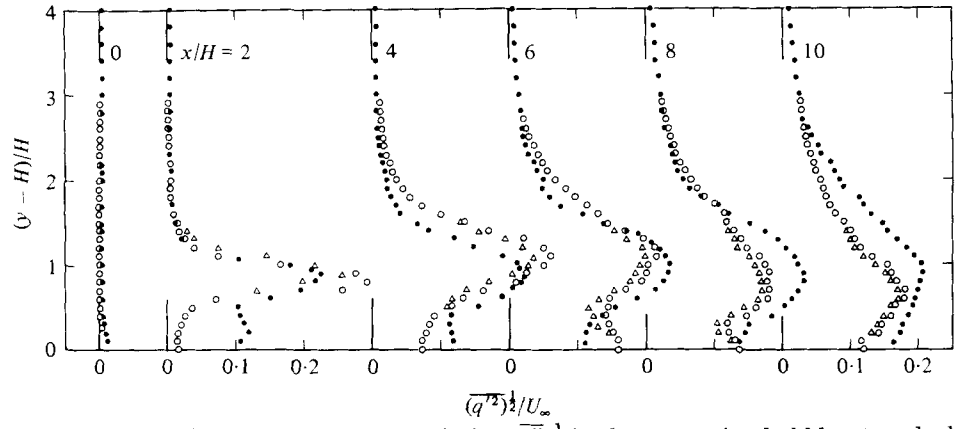

FIGURE 12. Distribution of the r.m.s. velocity $(\overline{q'^2})^{\frac{1}{2}}$ in the separation bubble. ○, calculation with $\sigma/H = 0{\cdot}05$; △, calculation with $\sigma/H = 0{\cdot}075$; ●, present experiment.

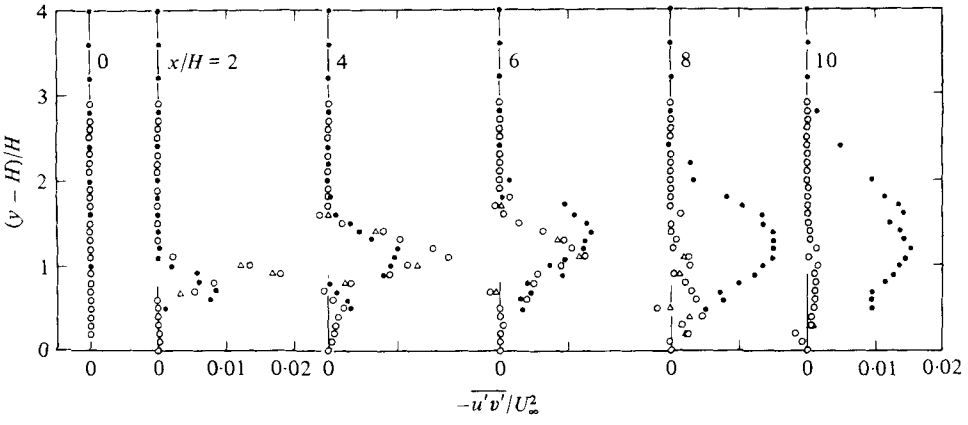

FIGURE 13. Distribution of Reynolds shear stress in the separation bubble. ○, calculation with $\sigma/H = 0{\cdot}05$; △, calculation with $\sigma/H = 0{\cdot}075$; ●, present experiment.

puted shear stress decreases rapidly near the reattachment point to a much lower level than the measured one. Moreover, the latter exhibits no sensible decrease there. A fairly good agreement between the calculated and measured profiles is observed only in the middle of the separation bubble. The same tendency of the Reynolds shear stress is also observed in a more elaborate discrete-vortex simulation of the flow downstream of a two-dimensional downward-facing step (Ashurst 1979*a*).

In our opinion, this feature of the computation is associated with the two-dimensional nature of the present discrete-vortex model. In the real flow, one may imagine that after separation a straight vortex parallel to the spanwise direction is formed. This straight vortex will not be stable to certain spanwise disturbances. If such a disturbance slightly deforms the vortex, the combination of the self-induction effect and non-uniform velocity distribution further deforms the vortex further downstream in such a way that it consists of a U-loop (see Hinze 1975, figure 6–31). One thus expects that streamwise components of the vortex develop, so that further downstream eddies with axes inclined in the x-direction occur, forming pairs with opposite signs of vorticity. These eddies will produce the fluctuating velocity components u'

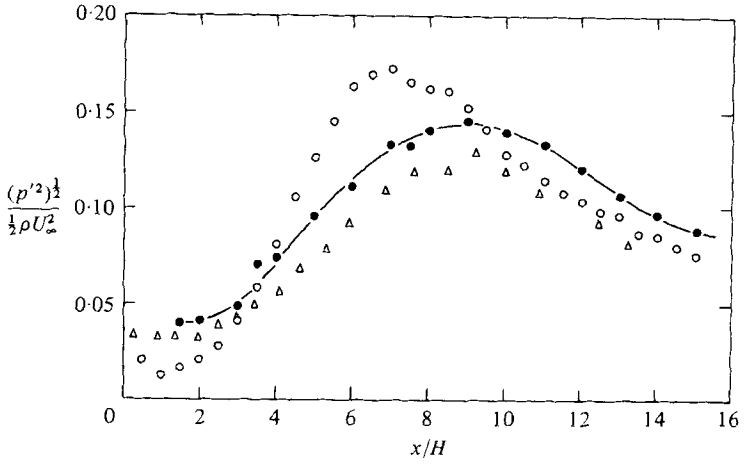

FIGURE 14. Distribution of the r.m.s. pressure along the surface of the plate. ○, calculation with $\sigma/H = 0{\cdot}05$; —●—, present experiment; △, experiment (with end plates) of Hillier & Cherry (1981). Line for visual aid only.

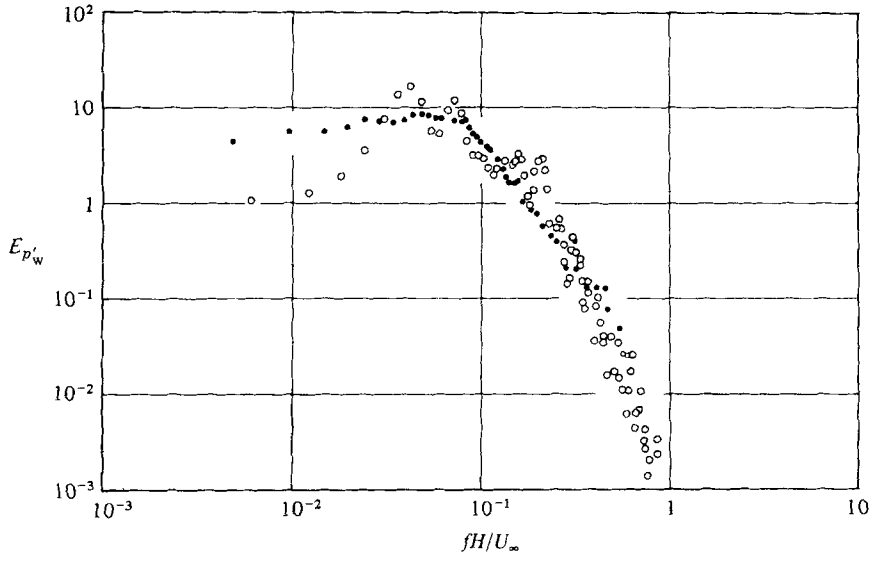

FIGURE 15. Power spectrum of surface-pressure fluctuation at $x/H = 10$. ○, calculation with $\sigma/H = 0{\cdot}05$; ●, present experiment.

and v', which are correlated very differently from those associated with the two-dimensional vortex clouds in the calculation. Figure 13 suggests that, in the real flow, the correlation $\overline{u'v'}$ may be contributed mainly by the deformed vortices near the reattachment zone. We imagine that the three-dimensional deformation of vortices may be significant there owing to certain intrinsic mechanisms and will probably lead to the eventual breakdown of vortices (see Clark & Kit 1980). In passing it may be noted that a fairly good agreement between the calculated and measured r.m.s. values of u' and v' does not generally guarantee a satisfactory result for the correlation $\overline{u'v'}$ between them.

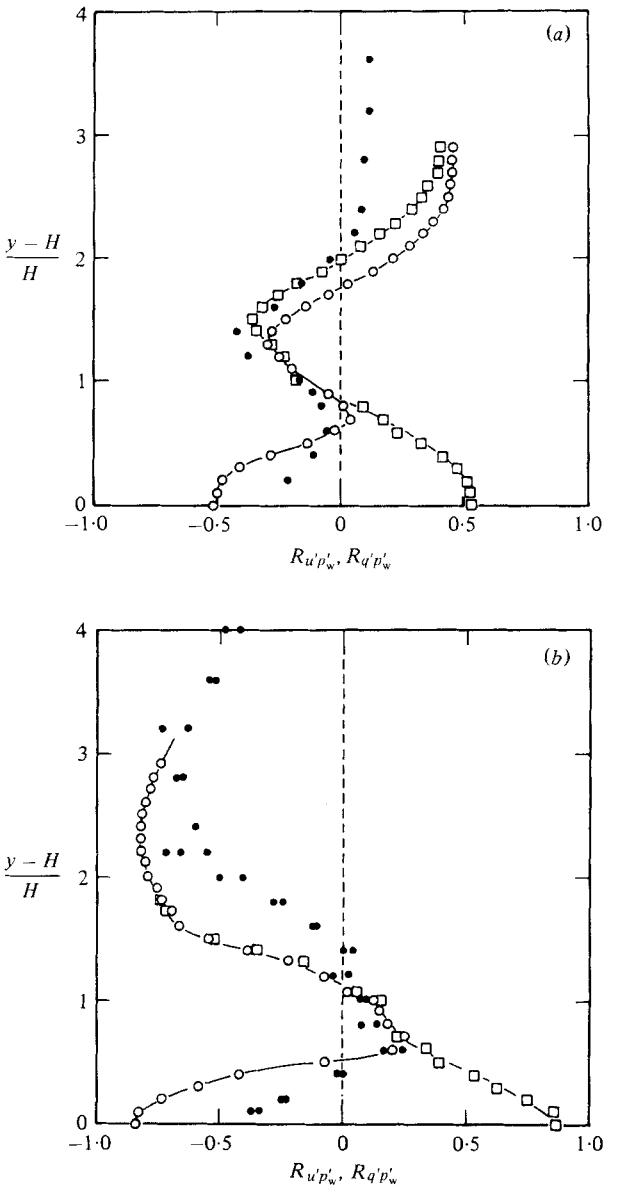

FIGURE 16(*a*, *b*). For caption see facing page.

The calculated and measured distributions of the r.m.s. values of the surface-pressure fluctuation p'_w are compared in figure 14. In both cases, a maximum r.m.s. pressure appeared at a position a little upstream of the time-mean reattachment point, which was $x/H = 9{\cdot}3$ and $9{\cdot}5$ for the calculation and the observation respectively. This feature is also observed by Wedding *et al.* (1978) on a separation–reattachment side of a square prism. The calculated maximum value was 20 % larger than the measured one.

The power spectrum of the surface-pressure fluctuations was obtained in the reattachment zone. The result at $x/H = 10$ is given in figure 15 in the form of $E_{p'_w}(f)$

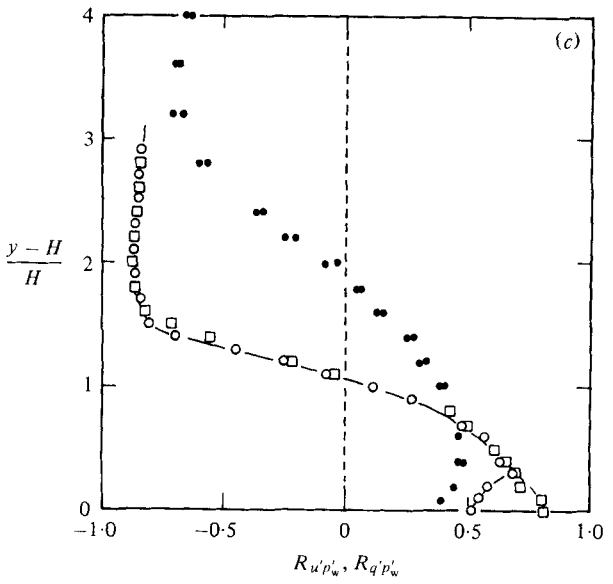

FIGURE 16. Distribution of the correlation coefficients between the surface-pressure and velocity fluctuations. ○, ●, $R_{q'p'_w}$; □, $R_{u'p'_w}$; open symbols for the calculation with $\sigma/H = 0{\cdot}05$ and filled circles for the experiment. (*a*) $x/H = 2$; (*b*) 6; (*c*) 10.

versus fH/U_∞, where f is the frequency and $E_{p'_w}$ denotes the one-sided spectrum defined by

$$\int_0^\infty E_{p'_w}(f)\,d(fH/U_\infty) = \overline{p'^2_w}/\tfrac{1}{2}\rho U_\infty^2.$$

The calculated and measured spectra are seen to be in reasonable agreement, except in the range of low frequencies. This result, however, may be considered as fortuitous because the calculated r.m.s. surface pressure at $x/H = 10{\cdot}0$ is not in excellent agreement with the experiment (see figure 14).

4.5. *Correlation between surface-pressure and velocity fluctuations*

In order to examine further the potentialities of the discrete-vortex model, correlations between the fluctuating surface pressure and the fluctuating velocities were calculated. The correlation $\overline{u'p'_w}$ has often been measured in wall-turbulence experiments because it is indicative of some features of large-scale vortex structures in such flows. Since the hot-wire measurement of u' and v' is difficult in highly turbulent regions, such as are found in the separation zone, the correlation $\overline{q'p'_w}$ was calculated and compared with the experimental result. As mentioned previously, q' will be measured more accurately than u'. Figure 16 shows the distribution of

$$R_{u'p'_w}\left[=\overline{u'p'_w}/(\overline{u'^2}\,\overline{p'^2_w})^{\frac{1}{2}}\right] \quad \text{and} \quad R_{q'p'_w}\left[=\overline{q'p'_w}/(\overline{q'^2}\,\overline{p'^2_w})^{\frac{1}{2}}\right]$$

as functions of the normal distance from the plate surface. A major difference between $R_{u'p'_w}$ and $R_{q'p'_w}$ appears in the reverse-flow region, beyond which they are almost identical except at the station $x/H = 2{\cdot}0$.

The calculated and measured results of $R_{q'p'_w}$ will be discussed in comparison. Apart from at the station $x/H = 2{\cdot}0$, the general shape of the correlation curves was

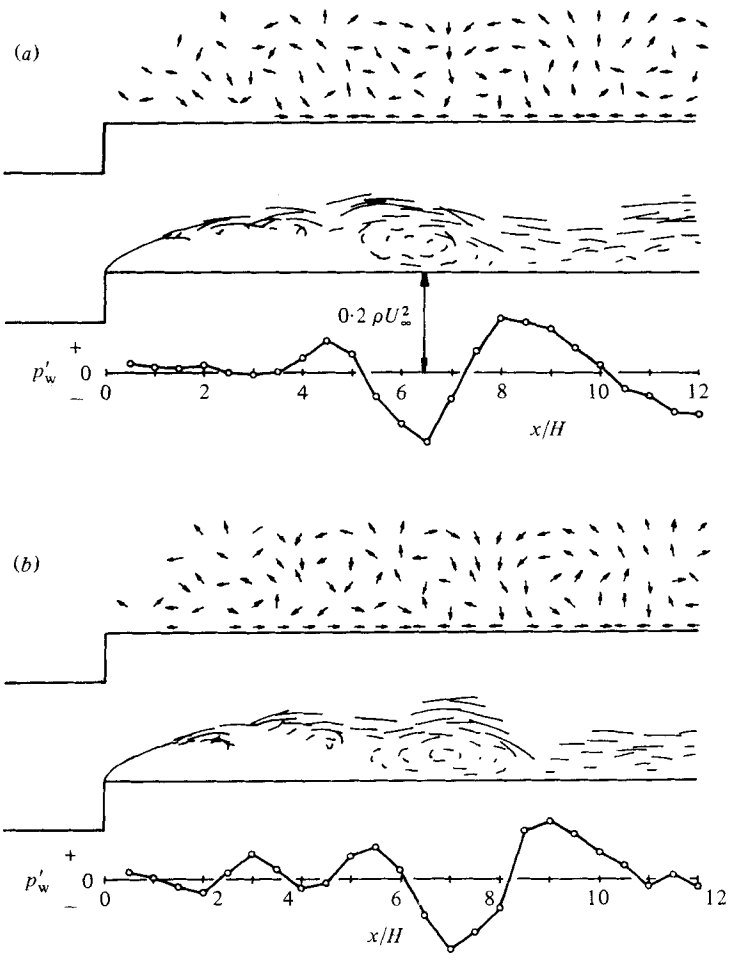

FIGURE 17 (*a*, *b*). For caption see facing page.

qualitatively similar, although there existed considerable quantitative differences between them, especially at the station furthest downstream of $x/H = 10$. That much smaller values of $R_{q'p'_w}$ were obtained nearer the plate surface in the experiment than in the calculation is explained by the no-slip condition at the surface; in the calculation, the fluctuating longitudinal velocity is non-zero there. A fairly good result for the station $x/H = 6$ suggests that the real-flow structure is well simulated in this region by the present discrete-vortex model. In other words, the two-dimensional large-scale vortex structures are mainly responsible for the fluctuating flow properties there. At the station further downstream at $x/H = 10$ the aforementioned three-dimensional deformation of vortices influences the correlation $R_{q'p'_w}$, so that the calculation yields less satisfactory results.

In the present experiment it was suspected that the shear layer a little downstream of the separation point exhibits an oscillating motion in the vertical direction with indefinite frequencies lower than roughly 50 Hz. The vertical motion is not evident in the calculation. In order to remove the effect of these fluctuations associated with

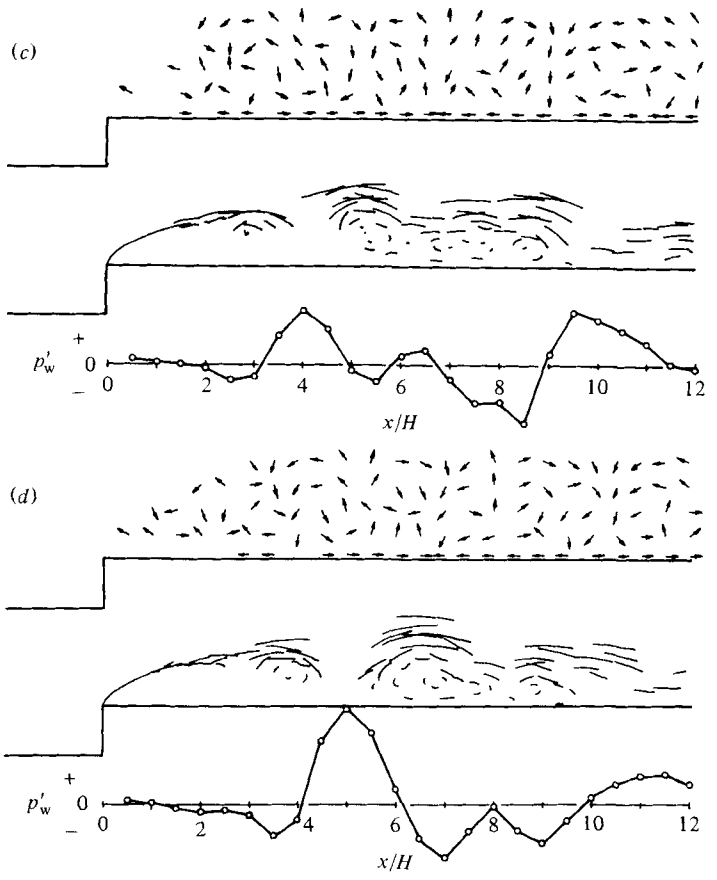

FIGURE 17. Instantaneous spatial distribution of the fluctuating components of surface-pressure and velocity vector. Trajectories of elemental vortices are shown during a time interval $0{\cdot}7H/U_\infty$ from the instant indicated. Note that only the direction of the fluctuating velocity vector is presented. (*a*) $U_\infty t/H = 88{\cdot}8$; (*b*) 90·7; (*c*) 92·6; (*d*) 94·6.

the said motion of the shear layer, the output of the hot wire and the pressure transducer were passed through a high-pass filter (50 Hz) before being fed to the signal processor. The resulting correlation profile is included in figure 16(*a*) to show that the agreement between the calculation and experiment is reasonable.

One now considers the correlation $R_{u'p'_w}$ in conjunction with the vortex patterns in the separation zone. Figures 16(*b*, *c*) indicate that this correlation is positive in the vicinity of the plate, and becomes negative when the distance y/H from the plate is larger than a certain value around 1·0. The vortex patterns in the separation bubble at several successive times are presented in figure 17, together with the instantaneous spatial variation of the fluctuating components of the surface pressure and the velocity vector. It may be noted that the arrows in these figures show only the direction of the velocity vectors and not their magnitude. In order to demonstrate the large-scale vortex patterns, figure 17 also includes the trajectories of elemental vortices during a short time interval $0{\cdot}7H/U_\infty$ with reference to a stationary co-ordinate. Although the vortex clouds are not very clear, their existence can be ascertained without much difficulty.

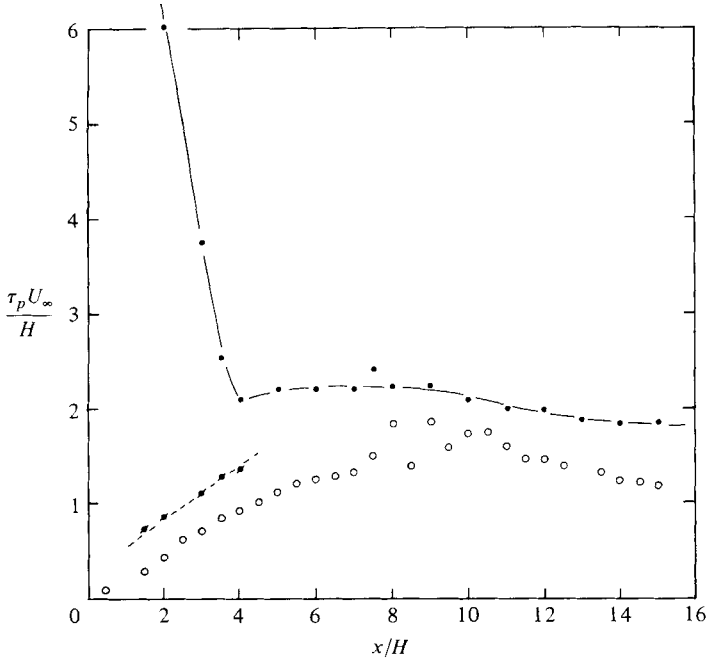

FIGURE 18. Distribution of integral time scale of the surface-pressure fluctuations. ○, calculation with $\sigma/H = 0{\cdot}05$; —●—, experimental result for overall frequencies; – – ● – –, experimental result for high-pass-filtered signal (50 Hz).

The fluctuating surface pressure is negative beneath the large-scale vortex clouds, whereas it is positive in regions where they are absent. As can be seen by looking progressively downwards in figure 17, the surface-pressure waveforms move in the downstream direction, approximately maintaining their general shapes. The corresponding peaks and valleys of the waveforms can be easily identified at each time. This demonstrates clearly that the spatial variation of the surface-pressure fluctuation is indicative of the large-scale structure in the flow. The fluctuating velocity component u' is generally negative in the lower part of any particular vortex cloud and positive in the upper part of it. On the contrary, in regions where the vortex clouds are absent, u' is positive in the vicinity of the plate and becomes negative beyond a certain distance from the plate. The aforementioned features of the fluctuating surface pressure and velocity are sufficient to explain the general shape of the correlation profiles $R_{u'p'_w} \sim y/H$ shown in figure 16.

After the present work was completed, a paper by Komatsu & Kobayashi (1980) came to our attention. They present the instantaneous pressure distribution along the sides of a transversely oscillating rectangular cylinder, the width being 3·0 times the height, together with the vortex pattern above the sides. Their results clearly demonstrate that the predicted relation between the instantaneous pressure distribution and the vortex pattern (figure 17) is correct.

Finally, the integral time scale τ_p of the surface-pressure fluctuation was evaluated from the autocorrelation coefficient $\overline{p'_w(x,t)\,p'_w(x,t+\tau)}/\overline{p'^2_w(x)}$, and plotted in figure 18 as a function of the longitudinal distance x/H. The experiment shows a steep increase of τ_p with decreasing x/H when $x/H < 4{\cdot}0$, whereas in the region $x/H > 4{\cdot}0$ the time scale is weakly dependent on the longitudinal distance. The large τ_p for $x/H < 4{\cdot}0$ is

considered to be attributable to the vertical oscillation of the shear layer mentioned previously. The pressure signals passed through the high-pass filter (50 Hz) were subsequently processed to yield an approximately linear increase of τ_p with increasing x/H in the region $x/H < 4{\cdot}0$. The resulting experimental variation of the time scale with x/H is qualitatively in fair agreement with the calculated result as shown in figure 18.

5. Concluding remarks

The discrete-vortex model has been utilized with some success to simulate the separation zone over a two-dimensional blunt flat plate with finite thickness and right-angled corners, which is aligned parallel to a uniform approaching stream. This flow situation is discriminated from other two-dimensional separated flows past bluff obstacles hitherto widely treated by this model in that no periodic vortex sheddings occur and, more importantly, the separated shear layer is strongly affected by the nearby solid surfaces.

A simple but effective procedure is employed to represent the effect of viscosity, which imposes the no-slip condition on the plate surface. A reduction in the circulation of elemental vortices is introduced as a function of their ages in order to represent partly the viscous and/or turbulent dissipation of vorticity, and partly the three-dimensional deformation of the vortex filaments, which leads to a decrease in the vorticity component normal to the plane of flow. Although the circulation reduction is inconsistent with the requirement that the angular momentum be conserved in inviscid flows, this can hardly be avoided to simulate adequately the overall structure of essentially dissipative flows. From the practical point of view, we feel that the circulation reduction is permissible if the resulting model can reveal some fundamental features of flow in the separation zone, which cannot easily be obtained by experimental means.

The present calculation yields a tolerable prediction of the time-mean and r.m.s. values of the velocity and surface-pressure fluctuations, together with the correlations between their fluctuating components, in the major part of the separation bubble. The interrelation between instantaneous large-scale vortex structures and instantaneous spatial variations of the surface-pressure and velocity fluctuations are also presented. A comparison between the calculated and measured Reynolds shear stress, however, indicates that in the real flow the three-dimensional deformation of vortex filaments becomes significant in the reattachment zone, so that the Reynolds shear stress cannot be well predicted there. Accordingly, in order to be more realistic, the discrete-vortex method should be extended to include the three-dimensional deformation of the vortex filaments. Finally, it should be remarked that no other analytical or numerical model has yet been able to produce equally satisfactory results for the separation-bubble flow at high Reynolds numbers.

The present study was supported by the Grant-in-Aid for Scientific Research from the Ministry of Education, Science and Culture of Japan. This paper was written while M. Kiya was a visitor in the Department of Applied Mathematics and Theoretical Physics, University of Cambridge, U.K. The authors express their sincere thanks to Mr T. Yamazaki and T. Sampo for their assistance in the construction of the experi-

mental apparatus, and to Mr H. Tamura and Dr Y. Suzuki for their valuable discussions and assistance in the manipulation of the data-processing apparatus. The authors also acknowledge Dr D. J. Maull and Dr J. C. R. Hunt for their kind comments and valuable discussion on an earlier version of the present paper. Finally our thanks are due to Mrs N. Coyle for her kindness in typing this manuscript.

REFERENCES

ACTON, E. 1980 A modelling of large eddies in an axisymmetric jet. *J. Fluid Mech.* **98**, 1–31.

AREF, H. & SIGGIA, E. D. 1980 Vortex dynamics of the two-dimensional turbulent shear layer. *J. Fluid Mech.* **100**, 705–737.

ASHURST, W. T. 1979*a* Calculation of plane sudden expansion flow via vortex dynamics. *Sandia Lab. Rep.* SAND 79–8679.

ASHURST, W. T. 1979*b* Numerical simulation of turbulent mixing layers via vortex dynamics. In *Turbulent Shear Flows I* (ed. F. Durst, B. E. Launder, F. W. Schmidt & J. H. Whitelaw), pp. 402–413. Springer.

ASHURST, W. T., DURST, F. & TROPEA, C. 1980 Two-dimensional separated flows: Experiment and discrete vortex dynamics simulation. *Sandia Labs Energy Rep.* SAND 79–8830.

BRADBURY, L. J. S. 1976 Measurements with a pulsed-wire and a hot-wire anemometer in the highly turbulent wake of a normal flat plate. *J. Fluid Mech.* **77**, 473–497.

CHORIN, A. J. 1973 Numerical study of slightly viscous flow. *J. Fluid Mech.* **57**, 785–796.

CLARK, J. A. & KIT, L. 1980 Shear layer transition and the sharp-edged orifice. *Trans. A.S.M.E.* I, *J. Fluids Engng* **102**, 219–225.

CLEMENTS, R. R. 1973 An inviscid model of two-dimensional vortex shedding. *J. Fluid Mech.* **57**, 321–336.

CLEMENTS, R. R. & MAULL, D. J. 1975 The representation of sheets of vorticity by discrete vortices. *Prog. Aerospace Sci.* **16**, 129–146.

EVANS, R. A. & BLOOR, M. I. G. 1977 The starting mechanism of wave-induced flow through a sharp-edged orifice. *J. Fluid Mech.* **82**, 115–128.

HILLIER, R. & CHERRY, N. J. 1981 The effects of stream turbulence on separation bubbles. *J. Wing Engng Ind. Aerodyn.* **8**, 49–58.

HINZE, J. O. 1975 *Turbulence*, 2nd edn. McGraw-Hill.

KIYA, M. & ARIE, M. 1977 A contribution to an inviscid vortex-shedding model for an inclined flat plate in uniform flow. *J. Fluid Mech.* **82**, 223–240.

KIYA, M. & ARIE, M. 1980 Discrete-vortex simulation of unsteady separated flow behind a nearly normal plate. *Bull. Japan Soc. Mech. Engrs* **23**, 1451–1458.

KOMATSU, S. & KOBAYASHI, H. 1980 Vortex-induced oscillation of bluff cylinders. *J. Wind Engng Ind. Aerodyn.* **6**, 335–362.

LEONARD, A. 1980 Vortex methods for flow simulation. *J. Comp. Phys.* **37**, 289–335.

NAGANO, S., NAITO, M. & TAKATA, H. 1981 Analysis of the flow past rectangular cylinders by the discrete-vortex method. *Trans. Japan Soc. Mech. Engrs* **47**, 32–43.

OTA, T. & ITASAKA, M. 1976 A separated and reattached flow on a blunt flat plate. *Trans. A.S.M.E.* I, *J. Fluids Engng* **98**, 79–86.

OTA, T. & KON, N. 1974 Heat transfer in the separated and reattached flow on a blunt flat plate. *Trans. A.S.M.E.* C, *J. Heat Transfer* **96**, 459–462.

OTA, T. & NARITA, M. 1978 Turbulence measurements in a separated and reattached flow over a blunt flat plate. *Trans. A.S.M.E.* I, *J. Fluids Engng* **100**, 224–228.

SARPKAYA, T. & SHOAF, R. L. 1979 Inviscid model of two-dimensional vortex shedding by a circular cylinder. *A.I.A.A. J.* **17**, 1193–1200.

TANI, I., IUCHI, M. & KODOMA, H. 1961 Experimental investigation of flow separation associated with a step or a groove. *Aeronautical Res. Inst., University of Tokyo, Rep.* no. 364.

WEDDING, J. B., ROBERTSON, J. M., PETERKA, J. A. & AKINS, R. E. 1978 Spectral and probability-density nature of square-prism separation–reattachment wall pressures. *Trans. A.S.M.E.* I, *J. Fluids Engng* **100**, 485–492.